Drug Design, Development and Therapy

Dovepress
Taylor & Francis Group

Open Access Full Text Article

ORIGINAL RESEARCH

Identifying Antihepatocellular Carcinoma Compounds in Gansui Banxia Decoction Using Live Cell Adsorption

Jiahao Huang[1,*], Hongyu Mao[1,2,*], Weidong Wu[3], Siliang Jiang[1], Lanru Chen[1], Tianyu Ma[1], Chunmei Zhai[3], Yonghai Meng[3]

[1]Key Laboratory of Basic and Application Research of Beiyao, Ministry of Education, Heilongjiang University of Chinese Medicine, Harbin, Heilongjiang, People's Republic of China; [2]Sinopharm Harbin General Hospital, Harbin, Heilongjiang, People's Republic of China; [3]Heilongjiang University of Chinese Medicine, Harbin, Heilongjiang, People's Republic of China

*These authors contributed equally to this work

Correspondence: Chunmei Zhai; Yonghai Meng, Heilongjiang University of Chinese Medicine, Harbin, Heilongjiang, 150040, People's Republic of China, Email zhaicm163@163.com; MengYonghai@outlook.com

Purpose: Gansui Banxia Decoction (GSBXD) is a traditional Chinese medicine formula for the treatment of hepatocellular carcinoma (HCC). Preliminary studies have identified the constituents and anticancer efficacy of GSBXD, but there is a gap in the screening of its lead compounds. Using live cell affinity combined with solid-phase extraction (LCA-SPE) and virtual screening and in vitro activity assays, we obtained 14 reliable potential lead compounds.

Methods: Coculturing H22 mouse HCC cells with GSBXD ethanol extract, isolating and purifying the bioactive fractions using LCA-SPE, and identifying the unknown bioactive components by ultraperformance liquid chromatography coupled with quadrupole time-of-flight full information tandem mass spectrometry (UPLC-QTOF-MS^E) with the UNIFI information processing platform were performed. Network pharmacology and molecular docking techniques predicted the potential mechanisms of these compounds against HCC. The enzyme-linked immunosorbent assay was used to examine the effects of core compounds on the expression of p53 and Bcl-2 in vitro.

Results: Fourteen compounds screened from GSBXD using SPE-LCA-UPLC-QTOF-MS^E may be the main bioactive components. Network pharmacology predictions suggested that protein kinases regulate Bcl-2 and p53 expression to trigger the apoptosis in cancer cells. Molecular docking identified three core compounds, namely, lactiflorin, schaftoside, and violanthin, which showed high affinities for the relevant proteins. Experimental verification confirmed their superior anticancer activity in vitro. Their anti-HCC effects likely involved in the upregulation of p53 and downregulation of Bcl-2 expression at the cellular level.

Conclusion: We developed a stable and accurate SPE-LCA method, which successfully isolated and characterized 14 potentially active compounds from GSBXD. They may improve HCC by promoting p53 expression and reducing Bcl-2 expression. This work lays a foundation for discovering lead compounds and exploring potential mechanisms in traditional Chinese medicine formulas.

Plain Language Summary: The search for bioactive compounds from herbal remedies remains one of the most challenging tasks in natural products chemistry. Herein, we developed an SPE-LCA-UPLC-QTOF-MS^E-based analytical procedure centered on the classic Chinese herbal formula Gansui Banxia decoction (GSBXD). This method used live mouse hepatocellular carcinoma (H22) cells as a stationary phase to screen for target compounds, which were enriched through a modified solid-phase extraction process and subsequently analyzed by LC-MS on the UNIFI platform. Using network pharmacology and molecular docking techniques, we further explored the potential antihepatocellular carcinoma (HCC) mechanisms of these compounds. This approach isolated and characterized 14 potentially active small molecules from the four GSBXD herbs. Preliminary validation indicated that their anti-HCC effects might be associated with the upregulation of p53 and downregulation of Bcl-2 at the cellular level. This method provides a reliable approach for screening lead compounds in complex herbal formulas, critical for advancing LCA-based analytical methods.

Keywords: Gansui Banxia decoction, UNIFI platform, UPLC-QTOF-MSE, solid-phase extraction, biospecific live cell-based isolation

Received: 24 December 2024
Accepted: 4 April 2025
Published: 29 April 2025

Graphical Abstract

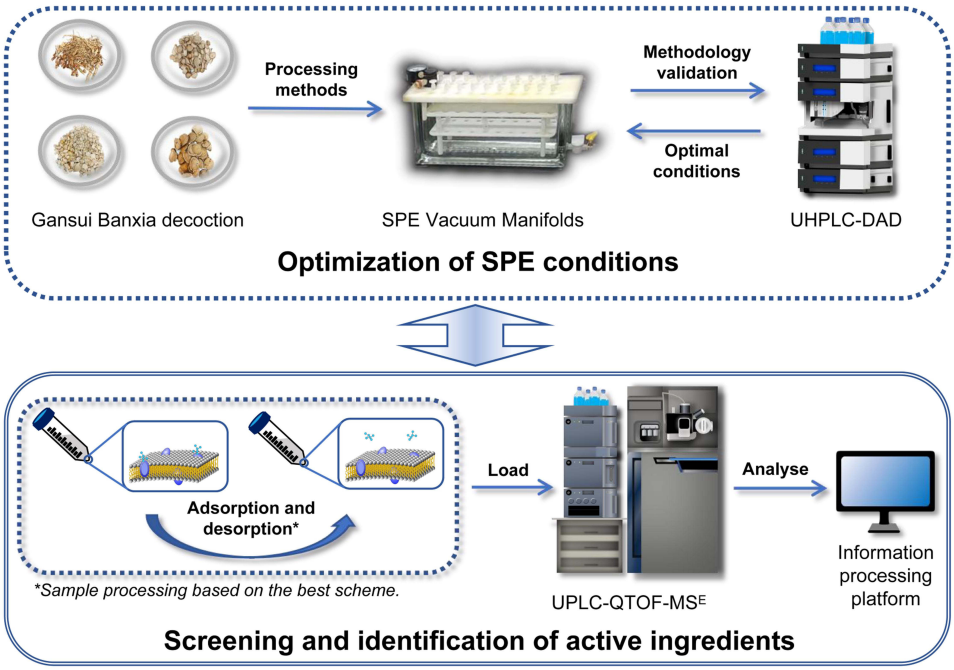

Introduction

Liver cancer is one of the most prevalent cancers. In particular, hepatocellular carcinoma (HCC) is the sixth most common cancer and the second leading cause of cancer deaths worldwide.[1] Despite the development of various treatment strategies for HCC, chemotherapy is still the primary treatment mode. Several targeted therapeutic agents, such as sorafenib and regorafenib, have been approved for HCC treatment. However, side effects and drug resistance often limit their therapeutic efficacy.[2,3] Therefore, the need for more effective anti-HCC therapies is urgent. Recently, extracts of traditional Chinese medicine and herbal formulas as potential treatments for HCC have become a considerable research focus. Gansui Banxia decoction (GSBXD), a traditional Chinese retained fluid-related disease formula, has gradually been investigated for HCC treatment.[4,5]

The use of GSBXD can be traced back to the beginning of the third century A.D. and is documented in the classic Chinese medicine book *The Essentials of the Golden Chamber* by Zhong-Jing Zhang. GSBXD comprises four traditional Chinese medicines (Table 1). It is important to note that the botanical names in the table are the accepted scientific names as found in the World Flora Online (www.worldfloraonline.org) as of March 27, 2024. GSBXD is a time-honored herbal formula employed in the clinical treatment of HCC.[6] Clinical observations have found that GSBXD can reduce tumor growth and slow cancer progression in patients diagnosed with HCC.[4,7] In animal studies, clinically equivalent doses of GSBXD did not show substantial toxicity to the liver and kidney.[5] Furthermore, through network pharmacology, a systems biology-based approach, combined with animal experiments, it was demonstrated that GSBXD can effectively inhibit the growth of HCC cell xenograft tumors in vivo and proteins such as Hsp90a, ATP1A1, and STAT3 are identified as potentially important in the treatment of HCC.[8] Additionally, the GSBXD extract has been shown to exert antitumor effects as an adjuvant therapy for HCC by inhibiting the accumulation and proliferation of MDSCs by inhibiting the AKT/STAT3/ERK signaling pathway.[9] Despite these findings, while specific mechanisms of GSBXD against HCC have been studied, the main active compounds of the overall formula have not been explored, making it impossible to clarify the primary mechanism of action.

Table 1 Chinese Medicinal Herbs Contained in the GSBXD

Botanical Plant Name	Chinese Name	Amount	Manufacturer Source	Batch Number
Euphorbia kansui Liou ex S.B.Ho	Gan Sui	15 g	Anguo Qicao Tang Herbal Slice Co.	D180801
Pinellia ternata (Thunb.) Makino	Ban Xia	30 g	Sichuan Jiangyou Zhongba Epiphyllum Technology Development Co.	20231002
Paeonia lactiflora Pall.	Bai Shao	15 g	Harbin Pufang Pharmaceutical Herbal Slice Co.	210401
Glycyrrhiza uralensis Fisch.	Zhi Gan Cao	7.5 g	Hebei Liankang Pharmaceutical Co.	2212013093

Drug discovery is an arduous process that involves a substantial amount of time and financial resources, and more importantly, it requires a vast pool of candidates to uncover a lead compound.[10] To address this challenge, researchers have developed various screening schemes for lead compounds.[11–13] Among these, cell membrane chromatography (CMC) has gained widespread use due to its simple preparation, low cost, and high sensitivity.[14–17] However, maintaining desired stability and lifetime for CMC is a technical challenge due to the irreversible nature of biofilm activity loss ex vivo and its detachment from the adsorption carrier.[15] Interestingly, based on the CMC principle, live cell adsorption (LCA) avoids this issue.[18] LCA not only eliminates the need for complex biofilm preparation procedures but also has specific stability and more bioconjugate-like conditions than simple CMC screening.[19] Additionally, solid-phase extraction (SPE) pretreatment techniques are widely used to prepare or enrich various natural products, biological samples, and hazardous substances.[20–24] Some researchers have screened the proangiogenic components of Buyang Huanwu decoction using biospecific live cell-based isolation combined with SPE.[18] This suggests that the SPE-LCA-UPLC-QTOF-MS^E screening system for discovery of lead compounds is feasible.

Based on the above studies, this study aimed to conduct a preliminary screening of bioactive components in GSBXD for HCC treatment by SPE-LCA-UPLC-QTOF-MS^E coupled with the UNIFI identification platform. The SPE conditions were meticulously optimized, and the samples treated with the best protocol were selected for analysis. The compounds were then virtually screened, and their mechanisms of action were predicted and validated. This study presents a reliable approach to screening active compounds in complex herbal formulations to treat HCC. Additionally, this is an attempt to discover lead compounds in complex herbal formula systems.

Materials and Methods

Materials and Reagents

Mouse hepatocellular carcinoma cells (H22) were purchased from BNCC (BeNa Culture Collection, Beijing, China). Fetal bovine serum was obtained from Biotopped (Biotopped Technology Corporation, Beijing, China). RPMI-1640 was purchased from Gibco (Invitrogen Corporation, Carlsbad, CA, USA). Penicillin–streptomycin double antibiotic solution was obtained from Sigma-Aldrich (St. Louis, MO, USA). The CCK-8 kit was purchased from Biosharp (Biosharp Biotechnology, Anhui, China). The BCA Protein Concentration Measurement Kit and RIPA lysis buffer were sourced from Beyotime (Beyotime Biotechnology, Shanghai, China). p53 and Bcl-2 enzyme-linked immunosorbent assay (ELISA) kits were purchased from Jingmei (Jiangsu Jingmei Biotechnology Corporation, Jiangsu, China). SPE-C18 and SPE-silica columns were purchased from Biocomma Co. MS-grade formic acid and acetonitrile were sourced from Thermo Fisher (Waltham, MA, USA). Ultrapure water was produced using a Millipore Milli-Q system (Bedford, MA, USA). All other chemical reagents used were analytical grade.

Preparation of GSBXD

The prescribed dosages of GSBXD are listed in Table 1. To prepare the GSBXD ethanol extract (GSBXD-EE), GSBXD medicinal herbs were totally immersed in anhydrous ethanol (*v*/*w*, 10:1) for 4 h and then heated to reflux at 80°C for 2 h. The filtrate was collected, and the residue was allowed to dry at 70°C for 12 h. Subsequently, the dried residue was extracted by hot reflux with 10 times the volume of anhydrous ethanol (*v*/*w*, 10:1) for 2 h. The anhydrous ethanol extract

solution was combined and concentrated to obtain the crude extract. Finally, the concentrated liquid was subjected to reduced pressure evaporation and lyophilized using an FDU-1200 freeze dryer (EYELA, Tokyo, Japan).

Optimization of SPE Conditions

To obtain better chromatograms and prolong the instrument's lifespan, the ideal SPE conditions should effectively remove inorganic salts and provide superior adsorption and desorption capabilities (ie, recovery) for the formula components. Recovery, as a critical factor in LCA sample processing, directly influences the identification of active compounds after dissociation. To achieve this, the optimization of conditions was demonstrated using an ultrahigh-performance liquid chromatography-diode array detection (UHPLC-DAD) system.

Pretreatment of Samples Before SPE

To prepare the working solution, lyophilized powder was dissolved in ethanol (0.2 g/mL), which was then separated using a D-101 macroporous adsorption resin column (2.6 cm i.d. × 30.0 cm), eluted with distilled water for 2 bed volumes (BV) until a negative Molisch reaction was observed, 30% (4.0 BV) EtOH to obtain the 30% EtOH eluent fraction (Fr. A), 60% (4.0 BV) EtOH solution to obtain 60% EtOH eluent fraction (Fr. B), and 90% (4.0 BV) EtOH solution to obtain 90% EtOH eluent fraction (Fr. C). The collected eluents (Fr. A, Fr. B, and Fr. C) were mixed, concentrated to 0.1 g/mL, and then filtered through a 0.22-μm membrane for spare use.

Chromatographic Conditions for UHPLC-DAD

Chromatographic separation for screening the SPE elution mode was performed using an UltiMate 3000 UHPLC system (Thermo Fisher Scientific Inc., Waltham, USA) equipped with a Kromasil C_{18} column (4.6 mm × 150 mm, 5.0 μm). The mobile phase was 0.1% formic acid in acetonitrile (A) and 0.1% formic acid in water (B) with the following gradient elution program: 0–1 min, 5%–18% A; 1–3 min, 18%–18.5% A; 3–10 min, 18.5%–30% A; 10–16 min, 30%–95% A; 16–18 min, 95%–95% A; 18–19 min, 95%–5% A; and 19–20 min, 5%–5% A. The column temperature was maintained at 30°C, the flow rate was 1.2 mL/min, the injection chamber temperature was maintained at 4°C, the injection volume was set to 2 μL, and the DAD detector scanned data across wavelengths from 200 to 700 nm, with appropriate wavelengths selected for data collection.

Selection of Optimal SPE Treatment Conditions

Two types of SPE columns with different separation characteristics were used: C_{18} (reversed-phase, RP) and silica (normal phase, NP). For forward elution (for RP): (A1) methanol; (B1) methanol containing 1% formic acid; (C1) acetonitrile; (D1) acetonitrile containing 1% formic acid. For reverse elution (for NP): (E1) n-hexane, (F1) n-hexane containing 5% ethyl acetate. The washing fluids used were water containing 5% methanol (A2-D2 by RP) and methanol (E2 and F2 by NP), with a total of six regimens of controlled conditions. The optimal conditions were selected by comparison of the resulting liquid chromatograms.

Six elution fractions (A1–F1) and six washing fluids (A2–F2) were collected and placed in a MG-2200 nitrogen blower (EYELA, Tokyo, Japan) to remove the solvents. The resulting samples were reconstituted in 200 μL of anhydrous ethanol and filtered through a 0.22-μm membrane to be subjected to the UltiMate 3000 UHPLC system. To ensure the reliability of the UHPLC method, injection of each sample should be repeated six times.

Selection of the Optimal Drug Delivery Regimen

The optimal drug delivery regimen was selected using a CCK-8 kit following the manufacturer's protocol. Briefly, H22 cells in the logarithmic growth phase were seeded into a 96-well plate (5000 cells per well). Lyophilized powders of the different extracts were dissolved in PBS (containing 0.1% DMSO). CCK-8 solution (100 μL/well) was added for 2 h and incubated for 12, 24, and 36 h. After incubation, optical density was measured at 450 nm with an Epoch2 microplate spectrophotometer (BioTek, Winooski, USA). Half-maximal inhibitory concentration (IC_{50}) was quantified using GraphPad Prism 8.0.

Live Cell Solid Chromatography

H22 cells were cultured in complete medium in 25 cm^2 flasks to a cell density of 1×10^6 cells/mL, centrifuged at 800 rpm for 5 min in a low-speed L420 centrifuge (Cence, Hunan, China) to discard the upper layer of the medium, washed and resuspended with an appropriate amount of PBS, and centrifuged again. Subsequently, the GSBXD-EE solution was added to adjust the drug concentration to 364.0 μg/mL. The solution was then incubated for 24 h and centrifuged, and the supernatant was discarded, resuspended, and rinsed with PBS, followed by centrifugation. This rinsing procedure was repeated six times, and the washing solution was collected each time after pretreatment. The blank group was also treated using the same process as above, except that no additional drug was added for incubation. Then, the drug solution was injected into the sample until there were no relevant peaks (by comparing with the blank group) in the UPLC-QTOF-MS^E. When injected into the sample, the rinsing was stopped. Next, 8 mL of sodium citrate buffer (pH = 4.0) was added for continued incubation. After 2 h, the blank control group was centrifuged, and the supernatant was collected for SPE. The resulting eluents from the dosing and blank groups were blown dry with nitrogen, dissolved in an appropriate amount of methanol by ultrasonication, and filtered through a 0.22-μm membrane for UPLC-QTOF-MS^E analysis.

Chromatography and MS Conditions

Chromatographic analysis was conducted on a Waters ACQUITY UPLC system (Waters Corporation, Milford, USA) equipped with a Waters ACQUITY UPLC HSS T3 column (2.1 mm × 100 mm, 1.8 μm) utilizing a mobile phase comprising 0.1% formic acid in acetonitrile (solution A) and 0.1% formic acid in aqueous solution (solution B) using the following gradient elution: 0–7 min, 1%–26% A; 7–14 min, 26%–50% A; 14–21 min, 50%–75% A; 21–28 min, 75%–99% A, 28.01 min, 99% A, 28.01–30 min, 99%–1% A. The column temperature was 30°C, the flow rate was 0.3 mL/min, the injection chamber temperature was 4°C, and the injection volume was 1 μL.

MS was performed on a Waters SYNAPT G2-Si Q-TOF mass spectrometer (Waters Corporation, Milford, USA) with an electrospray ionization (ESI) source in positive-ion mode with the following operating parameters: nebulizing and cone pore gases, nitrogen; capillary voltage, 3.0 kV; ion source temperature, 100°C; cone pore voltage, 40 V; ion source compensation voltage, 80 V; desolvation gas temperature, 250°C; cone pore gas flow rate, 50 $L\cdot h^{-1}$; desolvation gas flow rate, 600 $L\cdot h^{-1}$, collision energy, 30–40 eV; mass scanning range, 50–2000 Da; scanning interval, 0.014 s, data acquisition mode, MS^E. A LockSpray system was used for online mass calibration. The corrected markers were leucine-enkephalin and the positive ions. The calibration marker was leucine-enkephalin, the $[M + H]^+$ was 556.2771, and the flow rate of the calibration solution was 10 μL/min.

Component Analysis Method Based on the UNIFI Platform

A systematic search and collection of the chemical compositions of the four Chinese medicines in GSBXD were conducted through database searches, including PubMed (https://pubmed.ncbi.nlm.nih.gov/, accessed on Nov. 21, 2023), China National Knowledge Infrastructure (https://www.cnki.net/, accessed on Nov. 21, 2023), Traditional Chinese Medicine Systematic Pharmacology Database and Analysis Platform (https://old.tcmsp-e.com, accessed on Nov. 21, 2023), HERB (http://herb.ac.cn/, accessed on Nov. 21, 2023), Web of Science (https://www.webofscience.com, accessed on Nov. 21, 2023), MassBank (https://massbank.eu/MassBank/, accessed on Nov. 21, 2023), and ChemSpider (https://www.chemspider.com/, accessed on Nov. 21, 2023). The data collected included compound names, molecular formulas, precise molecular masses, and two-dimensional structural representations of the compounds. The collated GSBXD component library and the raw MS data were imported into the UNIFI platform to analyze the active components qualitatively. For data screening, the parameters were set as follows: the precise mass deviation was not more than 10 ppm, the detection limit of the high-energy peak intensity was set to 20.0 counts, and the low-energy peak intensity was set to 150.0 counts in three-dimensional (3D) peak detection. H^+ and Na^+ were selected as positive ions. The signal peaks with response values of not less than 1×10^4 counts were attributed to the analyses after excluding the typical peaks of the blank control. The filtered results were manually crosschecked with the database entries to exclude low-fitness items.

Network Pharmacology

Target Collection of Active Ingredients

Based on the screened active ingredients, target prediction was performed in the TCMSP database (https://old.tcmsp-e.com, accessed on Nov. 25, 2023), SEA database (https://sea.bkslab.org, accessed on Nov. 25, 2023), and SwissTargetPrediction database (http://www.swisstargetprediction.ch, accessed on Nov. 25, 2023). Targets with an estimated probability of being real (probability > 0.1) and meeting the requirements were screened out as the effective targets representing GSBXD.

Collection of HCC-Related Targets

We then conducted a search using "Hepatocellular carcinoma" as a keyword in the GeneCards database (https://www.genecards.org, accessed on Nov. 25, 2023), OMIM database (http://www.omim.org, accessed on Nov. 25, 2023), and TTD database (http://db.idrblab.net/ttd, accessed on Nov. 25, 2023). The relevant targets from all three databases were integrated, and duplicates were removed to compile a final collection of HCC-related targets. Finally, a Veen diagram was generated to illustrate shared targets as a collection of herbal and HCC targets.

Constructing the Protein–Protein Interactions (PPI) Network

The obtained active ingredient-related targets and HCC disease-related targets were imported into Venny 2.1.0 (https://bioinfogp.cnb.csic.es/tools/venny/, accessed on Nov. 25, 2023) to obtain the intersecting targets as potential anti-HCC targets. This provided the foundation for further analysis. We used the STRING database (https://www.string-db.org/, accessed on Nov. 25, 2023) and constructed a protein interaction network of protein–protein interaction (PPI) targets for HCC components. The network was imported into Cytoscape 3.9.1 for visualization and analysis and screened by the Centiscape 2.2 plug-in to identify the core targets of the active ingredients in HCC.

Gene Ontology Analysis and Kyoto Encyclopedia of Genes and Genomes Analyses

Gene Ontology (GO) and Kyoto Encyclopedia of Genes and Genomes (KEGG) enrichment analyses of the intersection targets were performed using the DAVID database (https://david.ncifcrf.gov/, accessed on Apr. 19, 2024). The resulting data were visualized by column charts and bubble charts using the analysis tools provided by the OmicStudio platform (https://www.omicstudio.cn/tool, accessed on Apr. 19, 2024).

Molecular Docking

The 3D structures of active small molecules were retrieved and downloaded from PubChem (https://pubchem.ncbi.nlm.nih.gov, accessed on Dec. 10, 2023). Target proteins were searched using UniProt (https://www.uniprot.org/, accessed on Dec. 10, 2023) to filter higher-resolution proteins for downloading. Nonpolar hydrogens in the small molecule ligands were merged using AutoDock 1.5.7, and the rotatable bonds and rotational centers in the structure were confirmed and then exported as PDBQT files. Free water molecules and cocrystallized ligands were removed with PyMol, stored as PDB files, and opened with AutoDock 1.5.7. Nonpolar hydrogens in the proteins were merged into the corresponding carbons, missing hydrogens and partial charges were added to the proteins, and the output was saved as PDBQT files.

AutoDock Vina software was used to locate the center of the docking site and adjust the docking pocket size to the appropriate position for blind docking,[25] and the spacing was set to 1 Å. Configuration files were exported, 14 small molecule ligands were rigidly docked to 9 protein receptors, and the binding sites and corresponding binding energies were calculated. Binding energy analysis was performed using heatmap plot tools in Hiplot Pro (https://hiplot.com.cn/, accessed on Dec. 10, 2023), a comprehensive web service for biomedical data analysis and visualization. The docking results were visualized using PyMol.

In vitro Anticancer Assay and ELISA for Active Compounds

The active compounds identified through screening were subjected to a CCK-8 in vitro activity assay to determine their IC_{50}. H22 cells were seeded in 6-well plates at a density of 1×10^6 cells per well, and each well was incubated with 0.1% DMSO and different concentrations of the active compounds for 24 h. The H22 cells incubated in complete medium containing 0.1% DMSO served as control. Following incubation, the cells were centrifuged, resuspended in

PBS, and centrifuged again. This washing process was repeated three times, and then, the cell precipitate was collected, placed on ice, and lysed using RIPA lysis buffer. The supernatant was centrifuged after 30 min, and then, the concentration was adjusted to obtain the final protein lysate to be tested. Protein concentration was measured using the BCA method. The expression of Bcl-2 and p53 in the cells was detected using ELISA kits, following the manufacturer's instructions.

Statistical Analysis

The experimental data are presented as mean ± standard error of the mean (SEM) for each group. Statistical analyses were conducted using GraphPad Prism (version 8.0). The data were subjected to Bartlett's test, and P-values > 0.05 were considered variance-aligned. Inter-group differences were assessed using one-way analysis of variance followed by Tukey's multiple comparison test to identify substantial differences between group means when overall P-value ≤ 0.05. A P-value < 0.05 was considered statistically substantial.

Results

SPE Condition Screening

The detection wavelength for the final UHPLC-DAD analysis was optimized to 250 nm. As shown in Figure 1A–F, the forward elution method applied to the reversed-phase chromatographic packing column proved to be more effective for the adsorption, enrichment, and desorption of the GSBXD components in this experiment. It is important to note that for subsequent UPLC-QTOF-MS^E detection, samples suitable are those eluted using both the forward and reverse elution methods. Although the eluent fractions from schemes E and F showed sharper and more prominent peaks in some cases compared to the other four schemes, the inorganic salts in the samples were also required to be removed by SPE in the present experiments, and the normal-phase silica packing column had a particular affinity for the inorganic salts. The subsequent methanol elution will cause most inorganic salts to desorb and flow out. Therefore, before moving forward with further experiments, we excluded schemes E and F and chose schemes A–D to continue the comparison of recovery rates to select the best scheme.

From the peak information in Table S1 and the histogram of the recoveries of the peaks of each scheme in Figure 1G and Table 2, peaks with a peak area of no less than 0.35 mAU·min were selected as common peaks for control. It was observed that 20 peaks could be detected at 250 nm in the precolumn sample. The four forward elution schemes were able to elute all the shared peaks. Schemes A and B show that the recoveries of the shared peaks could reach 24.07–124.84% when methanol was used as the primary eluent solvent. After optimizing the conditions, scheme B presented five peaks with recoveries greater than 80%. When acetonitrile with 1% formic acid was used as the eluent in scheme D, the recoveries were up to 26.04%–114.21%, and six peaks have recoveries greater than 80%. In contrast, the best recoveries could be obtained when pure acetonitrile was used as the eluent (scheme C), in the range of 46.70%–129.90%, and the recuperation of 12 peaks was more than 80%. In summary, it was experimentally verified that treatment scheme C could fully adsorb the target components while ensuring that the inorganic salts in the samples were removed as much as possible and that the eluent could desorb the bound packing material well. Therefore, scheme C was selected as the sample pretreatment method for the subsequent UPLC-QTOF-MS^E composition analysis.

Cell Viability Assays

The CCK-8 cell viability assay (Figure 2A) was performed, with 5-fluorouracil (5-FU) serving as a positive control for comparison (Figure 2B). GSBXD-EE reached the most sensitive inhibitory amounts (ie, IC_{50}) of H22 cells at drug concentrations of 690.9, 364.0, and 229.9 μg/mL at 12, 24, and 36 h dosing lengths, respectively. The IC_{50} values for 5-FU were 1658.0, 418.5, and 4.426 μM at 12, 24, and 36 h dosing lengths, respectively. Therefore, to minimize the interference of metabolites produced by the cells during treatment and to allow sufficient time for the cell membrane receptors to bind to the active compounds of the drug species, an incubation time of 24 h and a drug concentration of 364.0 μg/mL were selected as the optimal conditions for LCA experiments.

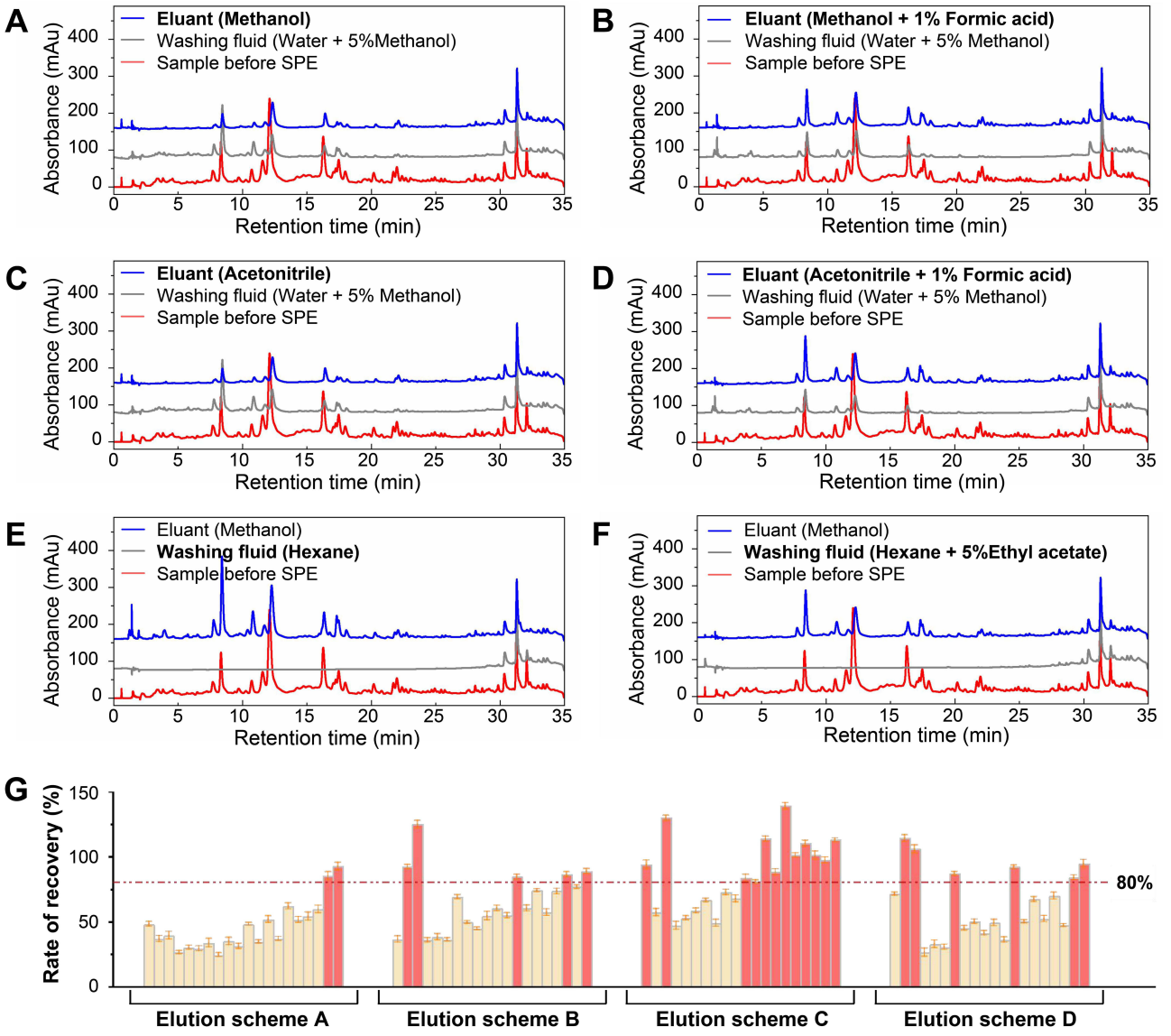

Figure 1 Effect of different washing and elution schemes on chromatographic peaks. (**A**). Washing by water plus 5% methanol and then eluting by methanol; (**B**). Washing by water plus 5% methanol and then eluting by methanol plus 1% formic acid; (**C**). Washing by water plus 5% methanol and then eluting by acetonitrile; (**D**). Washing by water plus 5% methanol and then eluting by acetonitrile plus 1% formic acid; (**E**). Washing by hexane and then eluting by methanol; (**F**). Washing by hexane plus 5% ethyl acetate and then eluting by methanol. Schemes A–D use the SPE-C18 column, while schemes E and F use the SPE-silica column. The red part of each individually stacked chromatogram is the crude extract of GSBXD-EE before SPE treatment, the gray parts are the fraction washed by different washing fluids, and the blue parts show the results of different elution fluids. Each component with a bold font is the target product to verify the result of condition optimization. (**G**). Recoveries of different SPE treatment protocols for the detected peaks. RSD < 3.5%.

Identification of LCA Dissociative Components

We used different controls for LCA treatment and UPLC-QTOF-MS^E detection after purification in combination with scheme C. In Figure 3A, several differential peaks were observed in the total ion chromatogram (TIC) plot of the dissociation solution (dissociation solution of blank control, DSB) of unadministered live cells compared to the sixth eluate (E-6) collected as blank reference. These peaks are likely caused by cellular secondary metabolites. Additionally, more complex signaling peaks were detected in the dissociation solution of administration (DSA) compared to DSB. Among them, an 8–15 min BPC plot (Figure 3B) was shown to better visualize the variability of ion intensity in each time point. After excluding common peaks, 14 differential peaks were identified for further analysis. This means that 14 compounds bound to the receptors in H22 cells were successfully dissociated. Subsequently, the initial screening and

Table 2 Chromatographic Peak Recoveries of Samples Obtained From Different SPE Treatment Protocols

Peak No.	Retention Time (min)	Recoveries of the Different Schemes (n = 6)							
		A		B		C		D	
		AVG	RSD	AVG	RSD	AVG	RSD	AVG	RSD
1	7.74	47.90%	1.81%	36.20%	2.50%	93.89%	3.20%	71.30%	1.27%
2	8.37	36.41%	2.44%	92.14%	1.57%	56.94%	2.89%	114.21%	2.65%
3	10.72	39.15%	2.91%	124.84%	3.02%	129.90%	1.95%	105.72%	3.22%
4	11.63	26.02%	1.23%	35.53%	1.70%	46.70%	3.05%	26.04%	3.20%
5	12.18	29.71%	1.59%	37.97%	2.42%	52.52%	1.61%	32.30%	2.91%
6	16.26	28.99%	1.98%	35.77%	1.39%	58.29%	1.84%	30.27%	1.99%
7	17.26	33.34%	3.21%	68.86%	1.61%	66.34%	1.38%	86.90%	1.49%
8	17.40	24.07%	1.48%	49.25%	1.07%	48.68%	2.79%	44.83%	1.73%
9	20.20	34.63%	2.79%	44.41%	1.02%	72.47%	2.10%	49.95%	1.62%
10	21.72	30.90%	1.98%	54.17%	3.28%	67.50%	2.61%	41.02%	1.65%
11	22.00	47.82%	1.01%	60.14%	2.06%	83.26%	2.94%	48.84%	2.47%
12	22.39	34.26%	1.35%	54.54%	1.96%	80.49%	1.48%	35.74%	2.15%
13	22.69	51.53%	2.51%	84.35%	1.93%	113.69%	2.00%	91.88%	1.48%
14	25.43	36.49%	1.45%	60.12%	2.29%	88.18%	2.34%	49.64%	1.24%
15	25.71	61.81%	2.23%	73.78%	1.16%	139.17%	2.57%	67.03%	1.82%
16	28.07	51.28%	2.25%	56.97%	2.58%	101.13%	1.76%	51.89%	2.40%
17	28.61	53.85%	3.14%	73.31%	2.19%	110.38%	2.29%	69.60%	2.59%
18	29.85	59.36%	2.79%	86.37%	1.76%	100.96%	3.25%	46.91%	1.10%
19	30.34	84.94%	3.22%	76.63%	1.32%	97.21%	2.44%	83.85%	1.79%
20	31.26	92.41%	3.03%	88.67%	1.93%	112.73%	1.59%	94.46%	3.02%

Abbreviations: AVG, Average; RSD, Relative standard deviation.

analysis of MS^E demonstrated specific fragmentation ion peaks through the UNIFI platform, with peaks 1, 2, 4, 9, 10, 11, 12, 13, and 14 identified as terpenoids and peaks 3, 5, 6, 7, and 8 identified as flavonoids.

The raw data were imported into the UNIFI platform for further analysis to identify the corresponding compounds (Table 3). The extracted ion chromatograms of these 14 compounds, the low-energy mass spectral information from the MS^E analytical mode, and the high-energy mass spectral information bar graphs were reprocessed and visualized using the UNIFI platform (Figure S1–S14). Compounds **3, 4**, and **5** were identified as schaftoside, lactiflorin, and violanthin,

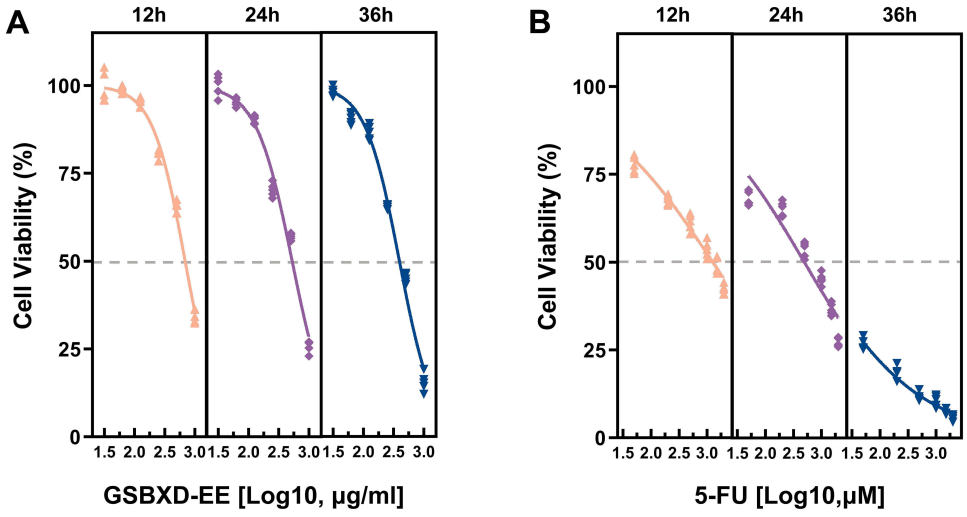

Figure 2 Effect of different drugs on H22 cell viability at different incubation times. (**A**) GSBXD-EE. (**B**) 5-FU. (n = 5).

https://doi.org/10.2147/DDDT.S513086

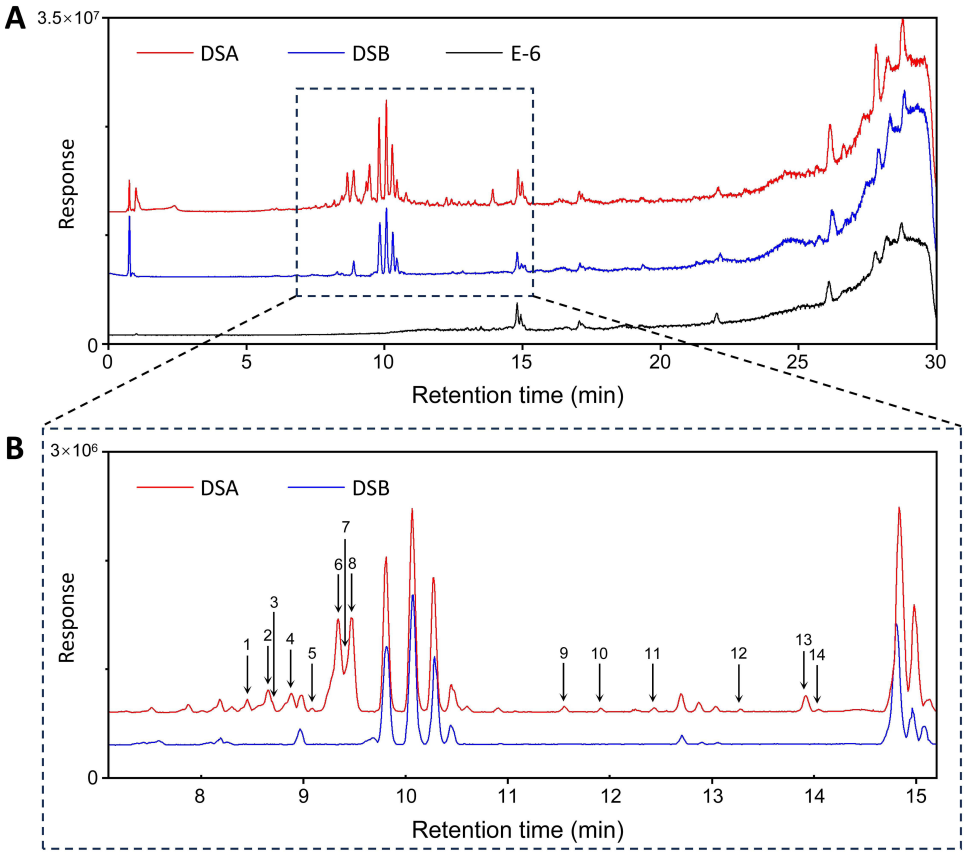

Figure 3 Chromatograms of the different components in positive-ion mode. (**A**) Complete TIC chart. (**B**) Localized magnified BPC plot.
Abbreviations: DSA, Dissociation solution of administration; DSB, Dissociation solution of blank control; E-6, the sixth-time elution solution.

respectively, by standard solution validation to support the subsequent experiments (Figure S15), including nine terpenoids and five flavonoids, of which nine compounds were derived from *Glycyrrhiza uralensis* Fisch, three were from *Paeonia lactiflora* Pall, and the other two were derived from *Euphorbia kansui* Liou ex S.B.Ho and *Pinellia ternata* (Thunb). Makino.

Flavonoids

The five flavonoids identified were all derived from *Glycyrrhiza uralensis* Fisch in GSBXD, in which the primary cleavage mode of the flavonoid glycosides in positive-ion mode was mainly glycosidic bond cleavage, such as loss of the neutral particle at 162 Da (Glc). In contrast, the retro Diels–Alder (RDA) cleavage pathway dominated the mass spectral behavior of the flavonoid glycosidic metabolites. Specifically, peak 6 was identified as a cleavage form described as pinocembrin, which was detected as the highest intensity peak of the adducted protonium ion at *m*/*z* 257.0804. In contrast, the structures predicted by the characteristic fragmentation ions at *m*/*z* 137.0231 (A1) and *m*/*z* 119.0488 (B1) also conform to the RDA cleavage pattern and also contain the fragment ion with the loss of neutral molecule H_2O at *m*/*z* 239.0697, so the structure of this compound is considered to be pinocembrin. The detailed mass spectral information for pinocembrin is presented in Figure 4.

Terpenoids

Nine terpenoids were identified from the four different herbs in the formula, mainly including monoterpenes and triterpene components, among others. For flavonoid glycosides, the glycosides formed by terpenoids were also first manifested in the breaking of the glycosidic bond under the bombardment of the ESI ion source, followed by successive loss of neutral small molecules after exposure of the glycosidic moiety. Two addition modes of synthesis were detected for peak 2 in positive-ion mode, namely, the addition of the proton-ion peak at *m*/*z* 503.1508 and the addition of the

Table 3 Identification of Binding Components in Dissociative Solutions Based on the UNIFI System Combined With UPLC-Q-TOF-MS^E

No.	$t_{(R)}$ (min)	Compound Name	Formula	Adduct ion	Observed *m/z*	Mass error (ppm)	MS^E	Herb
1	8.44	2′-(o,m-dihydroxybenzyl) sweroside	$C_{23}H_{26}O_{12}$	$[M + Na]^+$	517.1329	2.4	137.0231 $[M + H - C_{16}H_{21}O_9]^+$	*Ek*
2	8.65	Albiflorin	$C_{23}H_{28}O_{11}$	$[M + H]^+$ $[M + Na]^+$	481.1687 503.1508	−3.7	319.1167 $[M + H - Glc]^+$, 197.0804 $[M + H - Glc - C_7H_5O_2]^+$, 179.0699 $[M + H - Glc - C_7H_7O_3]^+$, 133.0645 $[M + H - Glc - C_8H_9O_5]^+$, 105.0329 $[M + H - Glc - C_{10}H_{13}O_5]^+$	*Pl*
3	8.70	Schaftoside*	$C_{26}H_{28}O_{14}$	$[M + H]^+$ $[M + Na]^+$	565.1521 587.1379	−5.5	481.2605, 379.0770	*Gu*
4	8.87	Lactiflorin*	$C_{23}H_{26}O_{10}$	$[M + H]^+$	463.1582	−3.6	301.1061 $[M + H - Glc]^+$, 179.0701 $[M + H - Glc - C_7O_2H_6]^+$, 151.0752 $[M + H - Glc - C_8O_2H_6]^+$	*Pl*
5	9.10	Violanthin*	$C_{27}H_{30}O_{14}$	$[M + H]^+$ $[M + Na]^+$	579.1690 601.1517	−3.2	417.1163 $[M + H - Glc]^+$	*Gu*
6	9.33	Pinocembrin	$C_{15}H_{12}O_4$	$[M + H]^+$	257.0804	−1.8	239.0697 $[M + H - H_2O]^+$, 137.0231 $[M + H - C_8H_8O]^+$, 119.0488 $[M + H - C_7H_6O_3]^+$	*Gu*
7	9.39	Naringenin	$C_{15}H_{12}O_5$	$[M + H]^+$	273.0753	−1.7	153.0179 $[M + H - C_8H_7O]^+$, 147.0438 $[M + H - C_6H_5O_3]^+$, 123.0435 $[M + H - C_8H_5O_3]^+$, 119.0488 $[M + H - C_7H_5O_4]^+$	*Gu*
8	9.47	Liquiritigenin	$C_{15}H_{12}O_4$	$[M + H]^+$	257.0804	−1.9	239.0700 $[M + H - H_2O]^+$, 147.0439 $[M + H - C_6H_5O_2]^+$, 109.0280 $[M + H - C_9H_7O_2]^+$	*Gu*
9	11.56	3-*O*-Benzoyl-20-deoxyingenol	$C_{27}H_{32}O_5$	$[M + H]^+$	437.2341	4.3	179.0698 $[M + H - C_{17}H_{21}O_2]^+$, 151.0748 $[M + H - C_{18}H_{21}O_3]^+$	*Pt*
10	11.91	Licoricesaponin A3	$C_{48}H_{72}O_{21}$	$[M + H]^+$ $[M + Na]^+$	985.4626 1007.4447	−1.3	809.4301 $[M + H - GlcA]^+$, 615.3873 $[M + H - 2\ GlcA]^+$, 453.3353 $[M + H - 2\ GlcA - Glc]^+$	*Gu*
11	12.43	Paeoniflorigenone	$C_{17}H_{18}O_6$	$[M + H]^+$	319.117	−2.0	301.1051 $[M + H - H_2O]^+$, 249.0748 $[M + H - C_4H_5O]^+$, 151.0752 $[M + H - C_8H_7O_4]^+$, 105.0332 $[M + H - C_{10}H_{13}O_5]^+$	*Pl*
12	13.28	Licoricesaponin G2	$C_{42}H_{62}O_{17}$	$[M + H]^+$ $[M + Na]^+$	839.4043 861.3858	−2.0	469.3303 $[M + H - 2\ GlcA]^+$, 451.3196	*Gu*
13	13.92	Glyyunnanprosapogenin D	$C_{42}H_{62}O_{16}$	$[M + H]^+$ $[M + Na]^+$	823.4091 845.3916	−2.4	647.3769 $[M + H - GlcA]^+$, 453.3352 $[M + H - 2\ GlcA]^+$, 189.1633, 149.0231, 119.0852	*Gu*
14	14.58	Licoricesaponin K2	$C_{42}H_{62}O_{16}$	$[M + H]^+$ $[M + Na]^+$	823.4093 845.3924	−2.1	647.3758 $[M + H - GlcA]^+$, 453.3350 $[M + H - 2\ GlcA]^+$, 191.0008, 207.0321	*Gu*

Notes: The asterisk means that a standard solution is already available for validation.
Abbreviations: Glc, glucose; GlcA, glucuronic acid; *Ek, Euphorbia kansui* Liou ex S.B.Ho; *Pt, Pinellia ternata* (Thunb.) Makino; *Pl, Paeonia lactiflora* Pall; *Gu, Glycyrrhiza uralensis* Fisch.

sodium-ion peak at *m/z* 481.1687. Both high- and low-energy levels exhibited sufficiently high response values, and the response value at *m/z* 319.1187 was sufficiently high and the loss of the neutral particle glucose was detected at *m/z* 319.1167, which in turn continued with the loss of the neutral small molecule benzoic acid at *m/z* 197.0804 and the exposure of the Glc parent nucleus continued with the loss of multiple neutral particles of H_2O and CO_2, as reflected in the *m/z* 179.0699 $[M - H_2O]^+$, *m/z* 161.0594 $[M - H_2O]^+$, and *m/z* 133.0646 $[M - H_2O - CO_2]^+$ fragmentation ion peaks. Based on the above fragmentation information, this compound was identified as the bitter pinane monoterpene glycoside albiflorin, and its detailed MS information and cleavage pathway are shown in Figure 5A and B. Meanwhile, the fragmentation information of peak 10 gave high-intensity ion peaks, mainly showing that the neutral particles GlcA (**I**) and Glc (**II**) were lost, which was identified as triterpene saponin licoricesaponin A3 by comparison with the other fragmentation information, and the mass spectral information is shown in Figure 6.

https://doi.org/10.2147/DDDT.S513086

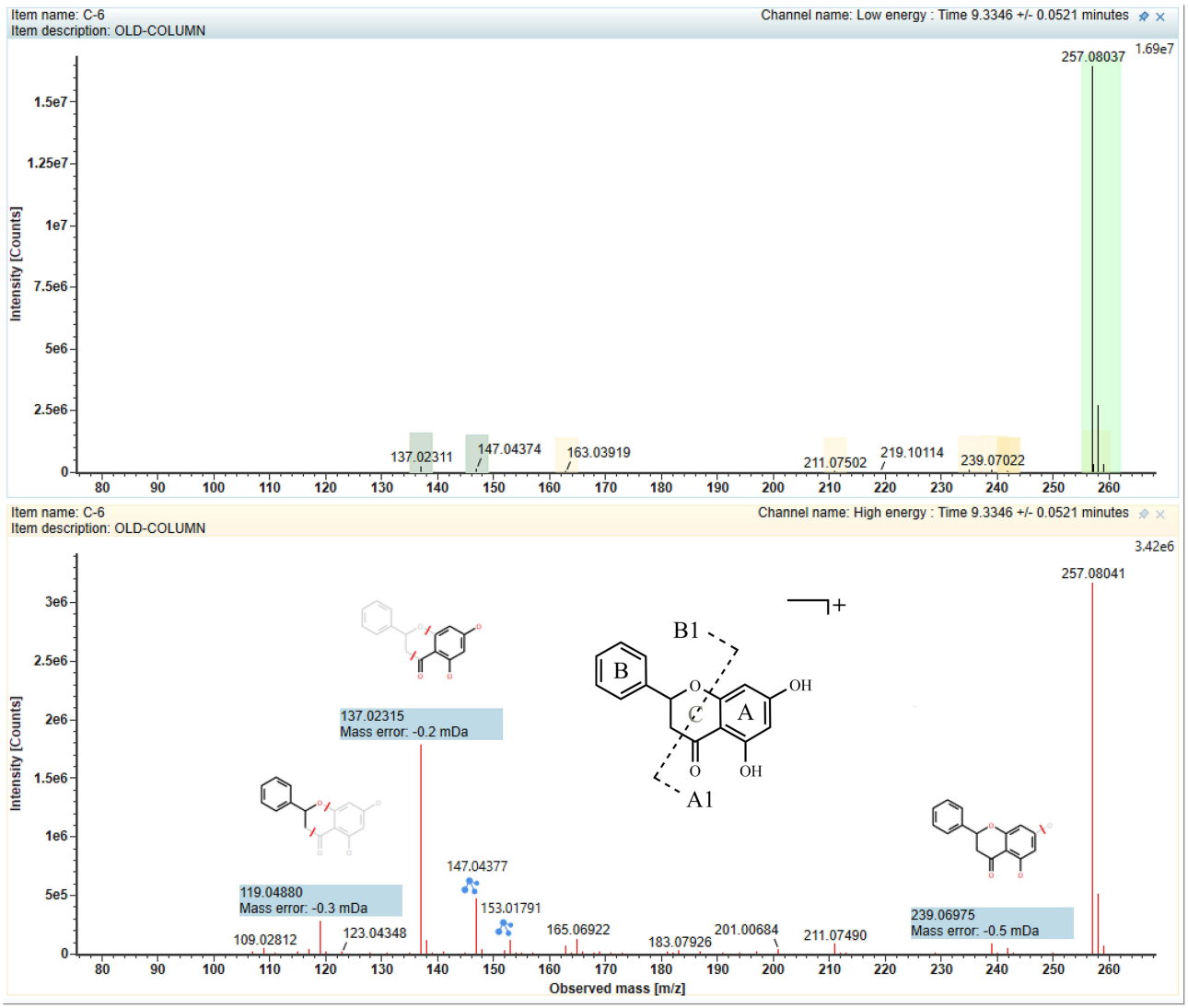

Figure 4 UNIFI-based identification process and fragmentation pathway of pinocembrin. MS/MS information at low/high energies and possible cleavage modes.

Analysis Based on Network Pharmacology and Molecular Docking Techniques

Construction of Drug-Disease Target Interaction Networks

In the TCMSP database, we matched 66 targets. In the SEA and SwissTargetPrediction databases, we predicted 240 and 564 targets, respectively. Individual Chinese medicine components were analyzed using a Veen diagram to delineate their relationships with the 14 compounds associated with HCC (Figure 7A), identifying 330 common targets. Based on the above targets to construct a PPI network, the targets were filtered with a degree greater than 14 to show that in the network graph (Figure 7B), each node represents a target and each edge represents the interaction between the two targets. The larger the area of a node and the darker the color, the larger its degree value; the darker the edge color, the higher the edge centrality. The key targets were predicted to be SRC, STAT3, EGFR, ESR1, PIK3CA, AKT1, PIK3CB, PIK3CD, and MAPK1 based on the degree value from high to low (Figure 7C).

GO and KEGG Pathway Enrichment Analysis

GO analysis showed 526 items related to anti-HCC efficacy ($P < 0.05$ and FDR < 0.05), comprising 367 biological processes (BP), 63 cellular components (CC), and 96 molecular functions (MF). The top 10 entries of *P*-values in BP, CC, and MF were visualized (Figure 8 A). We found that the *P*-values in BP and MF were substantially lower than those in CC, with protein phosphorylation playing a substantial role in BP. Notably, the MF entry was mainly associated with

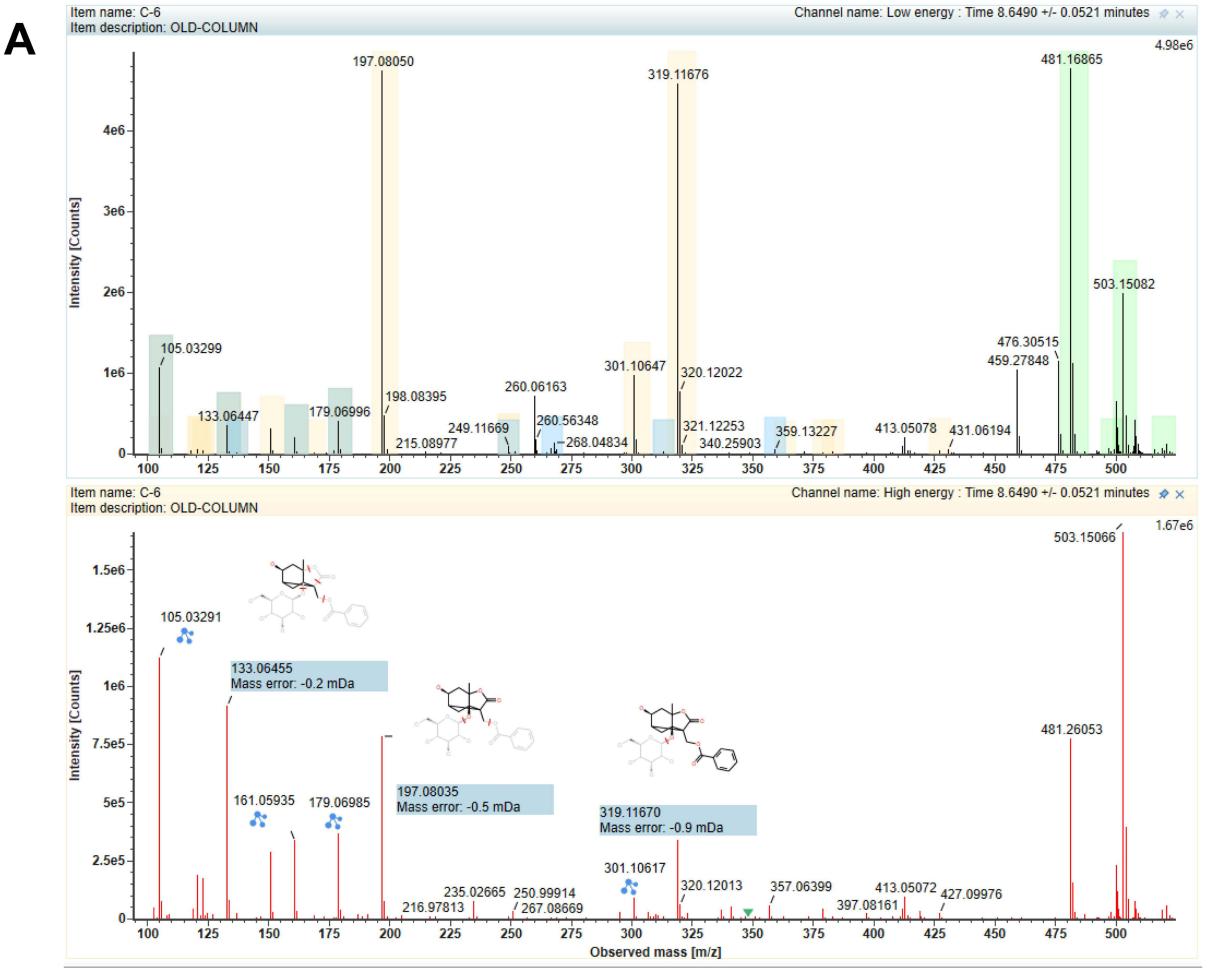

Figure 5 UNIFI-based identification process and fragmentation pathway of albiflorin. (**A**) MS/MS information and cleavage fragments at low/high energies. (**B**) Possible cleavage pathways.

https://doi.org/10.2147/DDDT.S513086

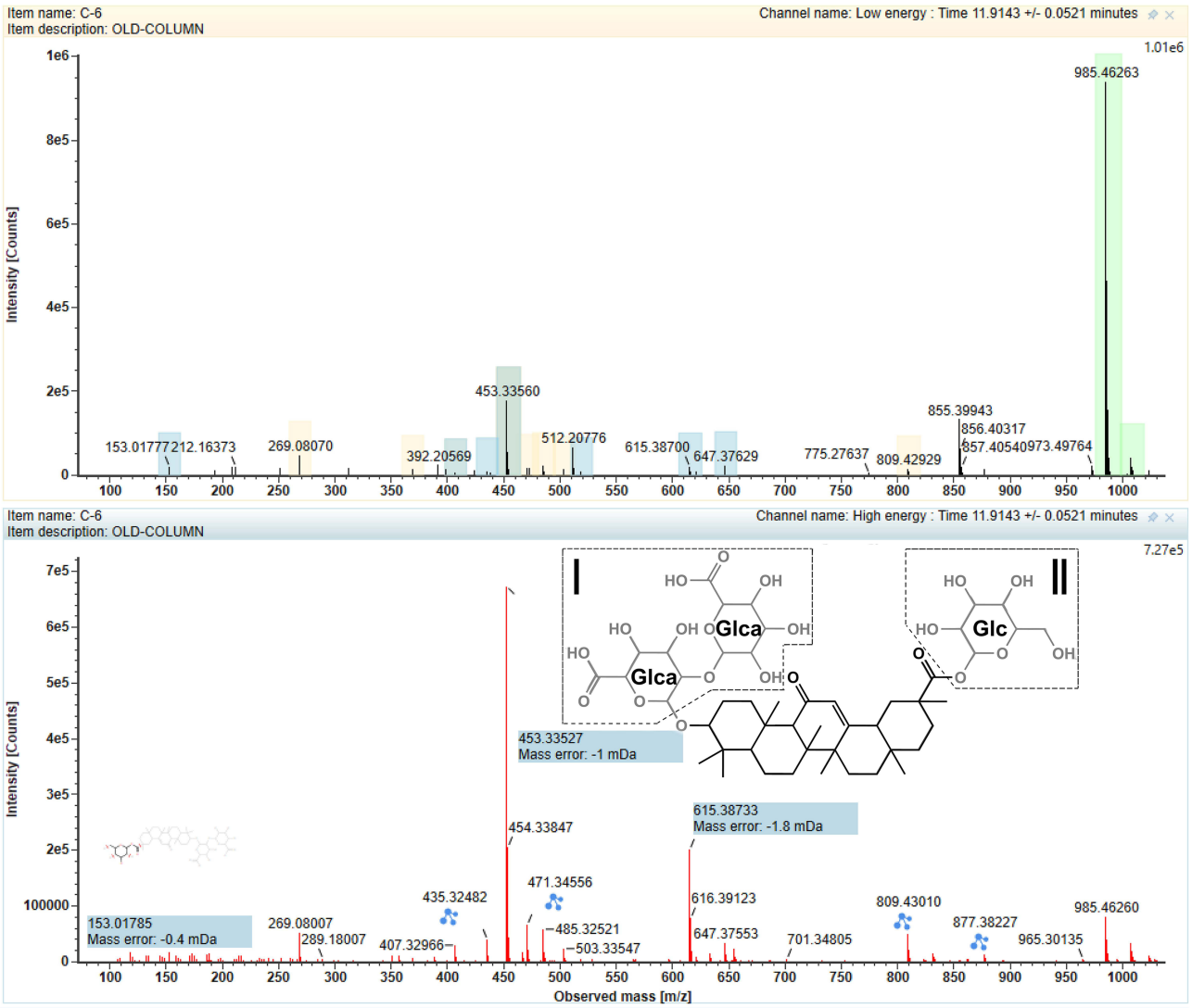

Figure 6 UNIFI-based identification process and fragmentation pathway of licoricesaponin A3. MS/MS information at low/high energies and possible cleavage modes.

protein kinase activity, ATP binding, enzyme binding, protein serine/threonine kinase activity, protein tyrosine kinase activity, protein kinase binding, identical protein binding, kinase activity, RNA polymerase II transcription factor activity, and ligand-activated sequence-specific DNA binding. This suggests that the anti-HCC mechanism of the active ingredients may be related to the regulation of multiple protein kinase activities. The KEGG pathway (Figure 8B) revealed that 176 were substantially enriched ($P < 0.05$ and FDR <0.05), and the *P*-value for the pathways in cancer was much smaller than those for the other pathways.

In summary, the active compounds may exert anticancer effects in the cancer pathway through various protein kinases, and we noticed that protein kinases regulate the expression of Bcl-2 and p53 to initiate the apoptotic program of cancer cells.[26,27] This relationship merits further experimental validation.

Docking Results of Active Compounds to Key Targets

Using AutoDock Vina, molecular docking of active small molecules with key targets was performed, and the molecular docking binding energy thermograms, as depicted in Figure 9A, ranged from 6.2 to −10.3 kcal/mol, demonstrating that the active small molecules exhibited excellent binding affinity to the core nodes. To explore in greater depth the interactions between active constituents and core targets, compounds exhibiting a strong binding affinity (less than or equal to −7.0 kcal/mol) to each core target were selected.[28] The top three small molecules, namely, schaftoside,

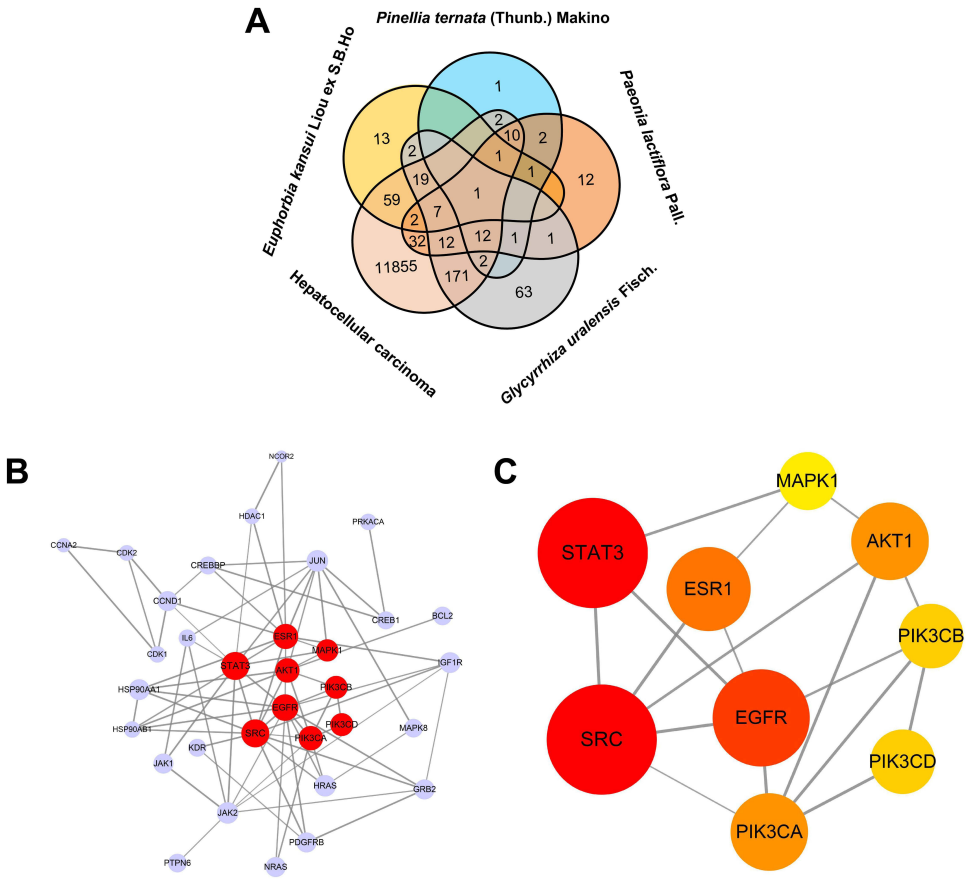

Figure 7 Drug-disease target enrichment. (**A**) Veen plot of the target intersection between TCM and HCC to which the active ingredient belongs. (**B**) Critical PPI network. (**C**) Core nodes of the critical PPI network. The size and color of a node are proportional to its degree value: the larger and brighter the node, the more critical the target in the network.

lactiflorin, and violanthin, were specifically chosen for their interactions with the key proteins in the PPI network, namely, STAT3, SRC, and EGFR. These interactions were visualized and are demonstrated in Figure 9B, indicating that the active ingredients screened by LCA-SPE have strong binding affinities to key targets associated with HCC. Molecular docking analysis underlines the potential of these compounds to interact with and modulate the activity of key targets, offering promising avenues for further exploration of their efficacy in HCC treatment. These three representative small molecules thus offer substantial insights into the molecular mechanisms underlying the efficacy of GSBXD in HCC treatment, emphasizing the need for additional experimental and clinical studies to validate these findings.

Additionally, studies have shown that SRC, STAT3, and EGFR can affect the expression of Bcl-2 and p53, which thus induces apoptosis in cancer cells.[29–31] Thus, the potential anticancer mechanisms of these three small molecules could be further explored by verifying their effects on the expression of Bcl-2 and p53 in vitro.

In vitro Anticancer Effects of Active Compounds and Related Protein Expression

The IC_{50} values of lactiflorin, schaftoside, and violanthin were 212.20, 95.60, and 52.85 μM, respectively, as determined by the CCK-8 and trypan blue exclusion assays (Figure S16).

Bcl-2, short for the B lymphoblastoma-2 gene, is a proto-oncogene that prolongs the cellular lifespan by inhibiting apoptosis, regulates mitochondrial dynamics, and regulates mitochondrial fusion and division. It has been shown that these effects help maintain the survival and proliferation of cancer cells.[32–35] As shown in Figure 10A, Bcl-2 expression was substantially increased in H22 cells without drug treatment. Bcl-2 expression was substantially reduced after incubation with different concentrations of lactiflorin, schaftoside, and violanthin in a dose-dependent manner ($P < 0.01$) compared to the control group.

https://doi.org/10.2147/DDDT.S513086

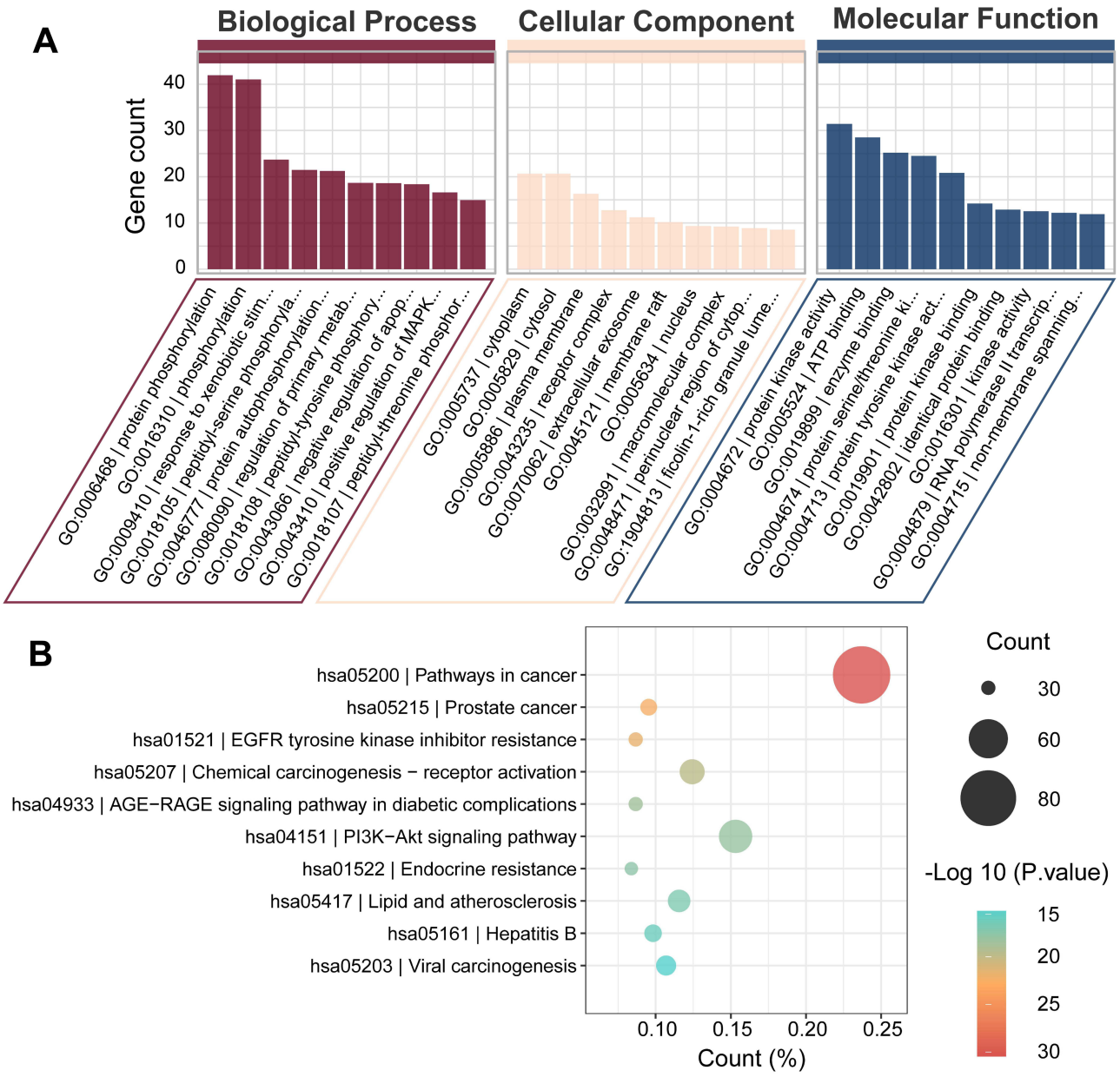

Figure 8 Gene enrichment analysis. (**A**) GO enrichment of the active compounds and HCC. (**B**) KEGG pathway enrichment of the active compounds and HCC.

p53 is a tumor suppressor gene through which the protein encoded by this gene controls the initiation of the cell cycle and is associated with cancer cell apoptosis. Studies have shown that the increased expression of p53 induces apoptosis in tumor cells and reduces the degree of carcinogenesis in normal cells to some extent.[36–38] As shown in Figure 10B, the expression of p53 was substantially increased after incubation with different concentrations of schaftoside compared to the control group without drug treatment. At the same time, violanthin and lactiflorin demonstrated more pronounced effects at medium and high concentrations ($P < 0.01$).

Discussion

The demand for herbal medicines has increased in recent years, and people have increasingly shifted from synthetic pharmaceutical drugs to naturally derived products.[39] Nowadays, a large number of clinical cases have proven that

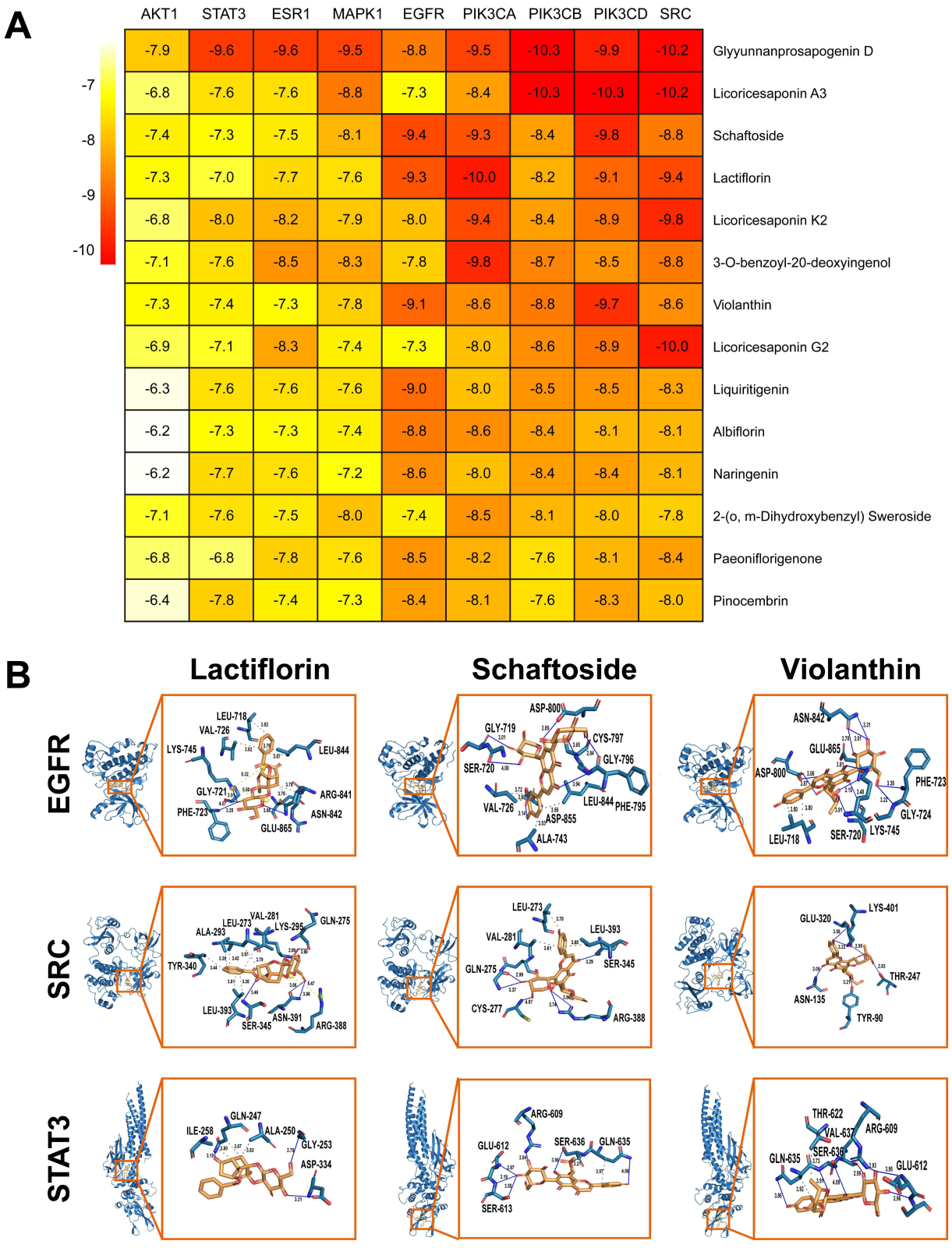

Figure 9 Molecular docking of active small molecules to core targets. (**A**) Heat map of molecular docking binding energy. (**B**) Visualization of docking of small molecules with strong binding affinity to key proteins. Models of lactiflorin, schaftoside, and violanthin binding to EGFR (PDB id: 8A2D), SRC (PDB id: 1FMK), and STAT3 (PDB id: 6NJS). In the binding model, hydrophobic interactions are represented by gray dashed lines, navy blue solid lines represent hydrogen bonds, yellow dashed lines represent salt bridges, and Orange dashed lines represent π–cation interactions.

https://doi.org/10.2147/DDDT.S513086

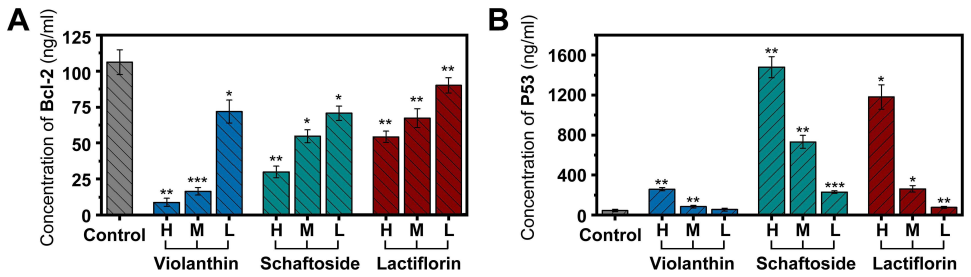

Figure 10 Effects of different active ingredients on the expression of specific apoptotic proteins in H22 cells. (**A**) Effect of different active ingredients on Bcl-2 expression in H22 cells. (**B**) Effect of different active ingredients on p53 expression in H22 cells. H, M, and L indicate high, medium, and low concentrations. The concentrations of lactiflorin were 428.4, 214.2, and 107.1 μM; those of schaftoside were 194, 97.3, and 48.65 μM; those of violanthin were 107.4, 53.7, and 26.85 μM, respectively. Values are expressed as mean ± SEM (n = 5). * P <0.05, ** P <0.01, *** P < 0.001, vs control group.

natural compounds with fewer side effects, such as hepatotoxicity, are not inferior to chemically synthesized drugs in terms of therapeutic efficacy.[40]

Therefore, the need to find effective lead compounds from herbal medicines has led to the birth of various isolation and screening techniques. Researchers have widely developed and utilized CMC due to its environmental friendliness and low use of chemical reagents to isolate compounds while ensuring their biological activity.[41] Despite these advantages, there are still many technical problems to be overcome in terms of stability and reproducibility of the system. However, the emergence of LCA avoids these problems by maintaining the integrity of the biofilm of living cells and the controllability of the cellular state.

Many of the existing LCA studies have been conducted based on multiple herbal formulas to explore their main active ingredients.[18,19] However, after a series of treatments and analyses, only several ingredients have been obtained, the number of which is less than that of herbal species in the formula. This contradicts the scientific basis of herbal formula combinations. In contrast, most CMC techniques tend to obtain richer results in screening active ingredients in formulas,[42] which is a technical challenge that LCA needs to urgently address.

To address this dilemma, we have optimized the general LCA method. First, the SPE-LCA-UPLC-QTOF-MS^E method used in our study increased the order of magnitude of the cells acted on in the pre-experimental screening, and we chose to culture them in suspension, which was effective in driving the binding components to a sizable concentration that can be captured by the UPLC-QTOF-MS^E system. Second, elution with multiple solvents from different SPE packing columns of different polarities reduced further loss of components during the enrichment of the dissociative components. We used an advanced MS^E information acquisition technique for the final component identification. This technique integrates the advantages of the three classical modes (full-scan, data-dependent, and data-independent acquisition), enabling the collection of more comprehensive fragment ion data. On this basis, access to the UNIFI data analysis platform reduces the analysis time and the possibility of human error in identifying compounds, making the results more credible.

While the SPE-LCA-UPLC-QTOF-MS^E method provided richer and more accurate results than other LCA methods currently available for obtaining lead compounds, there is still room for improvement. First, even if the research scope is limited to a particular disease, there are abundant cell lines, cell species, and phenotypes for investigation. This requires more theory and practice to support the feasibility of the LCA method and the representativeness of the selected cell lines. Second, some cells will be lost in the process of removing the interference of unbound components, which may interfere with the detection of some components in trace amounts. It is of interest to us the mechanism of action relationship among the lead compounds obtained from the screening and how they work together to change the state of the cells. This exploration can provide insights into the mechanism of action of the entire formula and that exploring the linkage of herbal formula pairing can be a strong basis for some of the pairing doctrines. In addition, the SPE method and MS setup can be further optimized. Finally, the limitations of this experiment are the virtual nature of blind docking and the partial nature of the validation screening results. Specifically, although blind docking saves cost and experiment time, there is still a huge potential for exploring the

actual binding of the compounds to the target. Moreover, the anti-HCC activity and the mechanism of action of other noncore potentially active compounds obtained by the LCA method need to be confirmed by research. To make the research more valuable, the toxicity, safety, and pharmacokinetics of these potentially active small molecules obtained through screening should be studied.

In summary, we propose a comprehensive SPE-LCA-UPLC-QTOF-MS^E screening system to screen and characterize the anti-HCC components of GSBXD. This strategy allows us to quickly locate potential compounds with pharmacological effects from an "ocean" of compounds and characterize them accurately. We expect that this system will be advantageous in the discovery of new lead compounds, the improvement of the quality control system of herbal medicines, and the exploration of unique formula mechanisms. This approach has broad potential applications in the biomedical fields, particularly in the development and design of new drugs.

Conclusion

This study established a biofilm separation method utilizing living cells as carriers. We used cancer cells as the research subject for the first time, combined with SPE and UPLC-QTOF-MS^E technology based on the UNIFI platform to screen the compounds with anti-HCC activities in complex TCM formulas. In the process, we identified 14 active ingredients extracted from four herbs. We used network pharmacology to screen the core targets SRC, STAT3, EGFR, ESR1, PIK3CA, AKT1, PIK3CB, PIK3CD, and MAPK1 for molecular docking. Among the screened compounds, we identified lactiflorin, schaftoside, and violanthin as potent protein-binding agents and found them to have good anti-HCC effects in vitro. All of them could promote p53 and reduce Bcl-2 expression. Our study showed that the active ingredients of GSBXD screened by LCA-SPE could effectively induce apoptosis in H22 hCC cells, exerting anticancer effects and improving HCC effects.

Abbreviations

5-FU, 5-Fluorouracil; Bcl-2, B-cell lymphoma-2; BP, Biological processes; BPC, Base peak chromatogram; BV, Bed volume; CC, Cellular components; CCK-8, Cell Counting Kit-8; CMC, Cell membrane chromatography; DSA, Dissociation solution of administration; DSB, Dissociation solution of blank control; E-6, The sixth eluent; ESI, Electrospray ionization; FBS, Fetal bovine serum; GO, Gene Ontology; GSBXD, Gansui Banxia decoction; GSBXD-EE, The ethanol extraction of Gansui Banxia decoction; HCC, Hepatocellular carcinoma; IC_{50}, 50% inhibitory concentration; KEGG, Kyoto Encyclopedia of Genes and Genomes; LCA, Live cell adsorption; LCA-SPE, Live cell affinity combined with solid phase extraction; LLE, Liquid-liquid extraction; MF, molecular functions; NP, Normal phase; P53, Tumor protein P53; RDA, Retro Diels-Alder; RP, Reversed phase; SPE, Solid phase extraction; TCM, Traditional Chinese medicine; TIC, Total ion flow chromatogram; UHPLC-DAD, Ultra-high performance liquid chromatography-diode array detection; UPLC-QTOF-MS^E, Ultra-performance liquid chromatography coupled with quadrupole time-of-flight full information tandem mass spectrometry; XIC, Extracted ion chromatogram.

Acknowledgments

This study was supported by grants of the Heilongjiang Postdoctoral Research Start-up Grant Funded Project (LBH-Q15137); Harbin Science and Technology Innovation Talent Research Special Fund Project (2017RAQXJ125); The establishment of innovative research projects for postgraduate students of Heilongjiang University of Chinese Medicine (2023yjscx040).

Disclosure

The authors report no conflicts of interest in this work.

References

1. Llovet JM, Kelley RK, Villanueva A, et al. Hepatocellular carcinoma. *Nat Rev Dis Primers*. 2021;7(1):6. doi:10.1038/s41572-020-00240-3

2. Vogel A, Meyer T, Sapisochin G, Salem R, Saborowski A. Hepatocellular carcinoma. *Lancet*. 2022;400(10360):1345–1362. doi:10.1016/s0140-6736(22)01200-4
3. Tang W, Chen Z, Zhang W, et al. The mechanisms of sorafenib resistance in hepatocellular carcinoma: theoretical basis and therapeutic aspects. *Signal Transduct Target Ther*. 2020;5(1):87. doi:10.1038/s41392-020-0187-x
4. Liu B, Sun N, Wang F. Clinical application of Gansui Banxia Tang. *Henan Traditional Chinese Medicine*. 2014;34(12):2297–2298. doi:10.16367/j.issn.1003-5028.2014.12.049
5. Liu H, Zhong Y, G S, et al. Effect of Gansui Banxia Tang plus-minus Gansui and Gancao anti-drug combination that preferred dose close to clinical application on diuretic effect in malignant ascites rats. *Zhongguo Zhong Yao Za Zhi*. 2014;39(14):2726–2731. doi:10.4268/cjcmm20141426
6. Wang Y, Sun Y, Li X, et al. Progress in the treatment of malignant ascites. *Crit Rev Oncol Hematol*. 2024;194:104237. doi:10.1016/j.critrevonc.2023.104237
7. Zhang A, Zhu F, M G, Deng F, He X, Zhou T,H. Xia Bin, director of the treatment of difficult cases 2 cases. *New Chinese Medicine*. 2013;45(10):169–170. doi:10.13457/j.cnki.jncm.2013.10.038
8. Zhang Y, Guo X, Wang D, et al. A systems biology-based investigation into the therapeutic effects of Gansui Banxia Tang on reversing the imbalanced network of hepatocellular carcinoma. *Sci Rep*. 2014;4:4154. doi:10.1038/srep04154
9. Feng XY, Chen BC, Li JC, et al. Gansui-Banxia decoction extraction inhibits MDSCs accumulation via AKT /STAT3/ERK signaling pathways to regulate antitumor immunity in C57bl/6 mice. *Phytomedicine*. 2021;93:153779. doi:10.1016/j.phymed.2021.153779
10. Han S, Lv Y, Wei F, Fu J, Hu Q, Wang S. Screening of bioactive components from traditional Chinese medicines using cell membrane chromatography coupled with mass spectrometry. *Phytochem Anal*. 2018;29(4):341–350. doi:10.1002/pca.2756
11. Hou X, Sun M, Bao T, Xie X, Wei F, Wang S. Recent advances in screening active components from natural products based on bioaffinity techniques. *Acta Pharm Sin B*. 2020;10(10):1800–1813. doi:10.1016/j.apsb.2020.04.016
12. McNair D. Artificial intelligence and machine learning for lead-to-candidate decision-making and beyond. *Annu Rev Pharmacol Toxicol*. 2023;63:77–97. doi:10.1146/annurev-pharmtox-051921-023255
13. Ramatapa T, Msobo A, Maphari PW, Ncube EN, Nogemane N, Mhlongo MI. Identification of plant-derived bioactive compounds using affinity mass spectrometry and molecular networking. *Metabolites*. 2022;12(9):863. doi:10.3390/metabo12090863
14. He X, Sui Y, Wang S. Application of a stepwise frontal analysis method in cell membrane chromatography. *J Chromatogr B Analyt Technol Biomed Life Sci*. 2020;1161:122436. doi:10.1016/j.jchromb.2020.122436
15. Fu J, Jia Q, Liang P, et al. Enhanced stability designs of cell membrane chromatography for screening drug leads. *J Sep Sci*. 2022;45(14):2498–2507. doi:10.1002/jssc.202200200
16. Wang N, Zhang Q, Xin H, Shou D, Qin L. Osteoblast cell membrane chromatography coupled with liquid chromatography and time-of-flight mass spectrometry for screening specific active components from traditional Chinese medicines. *J Sep Sci*. 2017;40(22):4311–4319. doi:10.1002/jssc.201700688
17. Liao F, He D, Vong CT, et al. Screening of the active Ingredients in Huanglian Jiedu decoction through amide bond-Immobilized magnetic nanoparticle-assisted cell membrane chromatography. *Front Pharmacol*. 2022;13:1087404. doi:10.3389/fphar.2022.1087404
18. Liao F, Meng Y, Zheng H, et al. Biospecific isolation and characterization of angiogenesis-promoting ingredients in Buyang Huanwu decoction using affinity chromatography on rat brain microvascular endothelial cells combined with solid-phase extraction, and HPLC-MS/MS. *Talanta*. 2018;179:490–500. doi:10.1016/j.talanta.2017.11.018
19. Yu A, Zheng H, Yan X, et al. Erythrocyte membrane affinity chromatography, solid-phase extraction and UPLC-QTOF-MS/MS to screen active ingredients of Buyang Huanwu decoction. *RSC Adv*. 2019;9(50):29217–29224. doi:10.1039/c9ra03447a
20. Cheng R, Mao X, Yu J, et al. A dispersive solid-phase extraction method for the determination of Aristolochic acids in Houttuynia cordata based on MIL-101(Fe): an analytes-oriented adsorbent selection design. *Food Chem*. 2023;407:135074. doi:10.1016/j.foodchem.2022.135074
21. Khatibi SA, Hamidi S, Siahi-Shadbad MR. Current trends in sample preparation by solid-phase extraction techniques for the determination of antibiotic residues in foodstuffs: a review. *Crit Rev Food Sci Nutr*. 2021;61(20):3361–3382. doi:10.1080/10408398.2020.1798349
22. Zou J, Yao B, Yan S, Song W. Determination of trace organic contaminants by a novel mixed-mode online solid-phase extraction coupled to liquid chromatography-tandem mass spectrometry. *Environ Pollut*. 2022;303:119112. doi:10.1016/j.envpol.2022.119112
23. Salim H, Pont L, Giménez E, Benavente F. On-line aptamer affinity solid-phase extraction direct mass spectrometry for the rapid analysis of α-synuclein in blood. *Anal Chim Acta*. 2023;1256:341149. doi:10.1016/j.aca.2023.341149
24. Maráková K, Renner BJ, Thomas SL, et al. Solid phase extraction as sample pretreatment method for top-down quantitative analysis of low molecular weight proteins from biological samples using liquid chromatography - triple quadrupole mass spectrometry. *Anal Chim Acta*. 2023;1243:340801. doi:10.1016/j.aca.2023.340801
25. Trott O, Olson AJ. AutoDock Vina: improving the speed and accuracy of docking with a new scoring function, efficient optimization, and multithreading. *J Comput Chem*. 2010;31(2):455–461. doi:10.1002/jcc.21334
26. Sidi S, Sanda T, Kennedy RD, et al. Chk1 suppresses a caspase-2 apoptotic response to DNA damage that bypasses p53, Bcl-2, and caspase-3. *Cell*. 2008;133(5):864–877. doi:10.1016/j.cell.2008.03.037
27. Soda G, Antonaci A, Bosco D, Nardoni S, Melis M. Expression of bcl-2, c-erbB-2, p53, and p21 (waf1-cip1) protein in thyroid carcinomas. *J Exp Clin Cancer Res*. 1999;18(3):363–367.
28. Abduljalil JM, Elfiky AA, Elgohary AM. Exploration of natural compounds against the human mpox virus DNA-dependent RNA polymerase in silico. *J Infect Public Health*. 2023;16(7):996–1003. doi:10.1016/j.jiph.2023.04.019
29. Berclaz G, Altermatt HJ, Rohrbach V, Siragusa A, Dreher E, Smith PD. EGFR dependent expression of STAT3 (but not STAT1) in breast cancer. *Int J Oncol*. 2001;19(6):1155–1160. doi:10.3892/ijo.19.6.1155
30. Karni R, Jove R, Levitzki A. Inhibition of pp60c-Src reduces Bcl-XL expression and reverses the transformed phenotype of cells overexpressing EGF and HER-2 receptors. *Oncogene*. 1999;18(33):4654–4662. doi:10.1038/sj.onc.1202835
31. Sp N, Kang DY, Lee JM, Bae SW, Jang KJ. Potential antitumor effects of 6-Gingerol in p53-dependent mitochondrial apoptosis and inhibition of tumor sphere formation in breast cancer cells. *Int J mol Sci*. 2021;22(9):4660. doi:10.3390/ijms22094660
32. Liu X, Dong J, Cai W, Pan Y, Li R, Li B. The effect of thymoquinone on apoptosis of SK-OV-3 ovarian cancer cell by regulation of Bcl-2 and Bax. *Int J Gynecol Cancer*. 2017;27(8):1596–1601. doi:10.1097/igc.0000000000001064

33. Bélanger S, Côté M, Lane D, L'Espérance S, Rancourt C, Piché A. Bcl-2 decreases cell proliferation and promotes accumulation of cells in S phase without affecting the rate of apoptosis in human ovarian carcinoma cells. *Gynecol Oncol*. 2005;97(3):796–806. doi:10.1016/j.ygyno.2005.02.018
34. Alhoshani A, Alatawi FO, Al-Anazi FE, et al. BCL-2 inhibitor venetoclax induces autophagy-associated cell death, cell cycle arrest, and apoptosis in human breast cancer cells. *Onco Targets Ther*. 2020;13:13357–13370. doi:10.2147/ott.S281519
35. Zhou J, Xia L, Zhang Y. Naringin inhibits thyroid cancer cell proliferation and induces cell apoptosis through repressing PI3K/AKT pathway. *Pathol Res Pract*. 2019;215(12):152707. doi:10.1016/j.prp.2019.152707
36. Marei HE, Althani A, Afifi N, et al. p53 signaling in cancer progression and therapy. *Cancer Cell Int*. 2021;21(1):703. doi:10.1186/s12935-021-02396-8
37. Schulz-Heddergott R, Stark N, Edmunds SJ, et al. Therapeutic ablation of gain-of-function mutant p53 in colorectal cancer Inhibits Stat3-mediated tumor growth and invasion. *Cancer Cell*. 2018;34(2):298–314.e7. doi:10.1016/j.ccell.2018.07.004
38. Kim J, Yu L, Chen W, et al. Wild-type p53 promotes cancer metabolic switch by inducing PUMA-dependent suppression of oxidative phosphorylation. *Cancer Cell*. 2019;35(2):191–203.e8. doi:10.1016/j.ccell.2018.12.012
39. Li K, Xiao K, Zhu S, Wang Y, Wang W. Chinese herbal medicine for primary liver cancer therapy: perspectives and challenges. *Front Pharmacol*. 2022;13:889799. doi:10.3389/fphar.2022.889799
40. Rani J, Dhull SB, Rose PK, Kidwai MK. Drug-induced liver injury and anti-hepatotoxic effect of herbal compounds: a metabolic mechanism perspective. *Phytomedicine*. 2024;122:155142. doi:10.1016/j.phymed.2023.155142
41. Ma W, Wang C, Liu R, et al. Advances in cell membrane chromatography. *J Chromatogr A*. 2021;1639:461916. doi:10.1016/j.chroma.2021.461916
42. Tang YP, Xu DQ, Yue SJ, Chen YY, Fu RJ, Bai X. Modern research thoughts and methods on bio-active components of TCM formulae. *Chin J Nat Med*. 2022;20(7):481–493. doi:10.1016/s1875-5364(22)60206-1